Journal of Applied Physics

AIP Publishing

Temperature sensing with RF-dressed states of nitrogen-vacancy centers in diamond

Hibiki Tabuchi,[1,2] Yuichiro Matsuzaki,[3] Noboru Furuya,[1] Yuta Nakano,[4] Hideyuki Watanabe,[3] Norio Tokuda,[4,5] Norikazu Mizuochi,[6] and Junko Ishi-Hayase[1,2]

[1)]*School of Fundamental Science and Technology, Keio University, Yokohama, Kanagawa 223-8522, Japan*
[2)]*Center for Spintronics Research Network, Keio University, Yokohama, Kanagawa 223-8522, Japan*
[3)]*National Institute of Advanced Industrial Science and Technology (AIST), Tsukuba, Ibaraki 305-8568, Japan*
[4)]*Graduate School of Natural Science and Technology, Kanazawa University, Kanazawa, Ishikawa 920-1192, Japan*
[5)]*Nanomaterials Research Institute, Kanazawa University, Kanazawa, Ishikawa 920-1192, Japan*
[6)]*Institute for Chemical Research, Kyoto University, Uji, Kyoto 611-0011, Japan*

(*Author to whom correspondence should be addressed: hayase@appi.keio.ac.jp)

(*Author to whom correspondence should be addressed: matsuzaki.yuichiro@aist.go.jp)

(Dated: 3 December 2022)

Using the electronic spin of nitrogen-vacancy (NV) centers in diamond is a promising approach to realizing high-precision temperature sensors; furthermore, pulsed optically detected magnetic resonance (pulsed-ODMR) is one way to measure the temperature using these NV centers. However, pulsed-ODMR techniques such as D-Ramsey, thermal echo, or thermal Carr–Purcell–Meiboom–Gill sequences require careful calibration and strict time synchronization to control the microwave (MW) pulses, which complicates their applicability. Continuous-wave ODMR (CW-ODMR) is a more advantageous way to measure temperature with NV centers because it can be implemented simply by continuous application of a green laser and MW radiation. However, CW-ODMR has lower sensitivity than pulsed-ODMR. Therefore, it is important to improve the temperature sensitivity of CW-ODMR techniques. Herein, we thus propose and demonstrate a method for measuring temperature using CW-ODMR with a quantum spin state dressed by a radio-frequency (RF) field under a transverse magnetic field. The use of an RF field is expected to suppress the inhomogeneous broadening resulting from strain and/or electric-field variations. The experimental results confirm that the linewidth is decreased in the proposed scheme when compared to the conventional scheme. In addition, we measured the temperature sensitivity to be about 50.4 ± 3.5 mK$/\sqrt{\text{Hz}}$, and this is approximately eight times better than that of the conventional scheme.

I. INTRODUCTION

With continuing advances in technology, there is an ongoing need to investigate matter at ever smaller scales. In particular, thermal effects play important roles at very small and localized scales. Therefore, measuring the local temperature with high sensitivity and high spatial resolution is of paramount importance to investigating the properties of cells[1–3] and nanodevices.[4–6]

A nitrogen-vacancy (NV) center in diamond is a defect in which two adjacent carbon atoms are replaced by a nitrogen atom and a vacancy.[7,8] Since the electron spin resonance frequency of an NV center is temperature dependent, it can be used as a temperature sensor.[9] NV centers have a long spin-coherence time of a few milliseconds for high-sensitivity measurements[10–12] and can be incorporated into nanodiamond probes as small as tens of nanometers for high-spatial-resolution measurements.[13–15] Moreover, as temperature sensors, NV centers have a wide dynamic range from hundreds to thousands of kelvin.[16–18] Given these properties, using NV centers represents a promising approach to realizing high-sensitivity and high-spatial-resolution temperature sensors.[4,8,10,16,17,19]

One way to measure temperature with NV centers is to use pulsed-optically detected magnetic resonance (pulsed-ODMR) techniques such as D-Ramsey, thermal echo, or thermal Carr–Purcell–Meiboom–Gill sequences.[20–23] Pulsed-ODMR measurements create a superposition of quantum states in which a change in temperature induces an additional phase in the superposition. The temperature can thus be estimated by detecting this phase shift via optical measurements. Although pulsed-ODMR generally provides high temperature sensitivity, it requires careful calibration, including strict time synchronization to control microwave (MW) pulses.

Continuous-wave ODMR (CW-ODMR) is another method for measuring temperature using NV centers.[1–3,24,25] Temperature changes induce shifts in the NV spin-resonance frequency, and these can be measured from the CW-ODMR spectrum. Temperature sensing by CW-ODMR is advantageous because it is simple to perform through the continuous application of a green laser and an MW field without the need complicated calibration. In addition, CW-ODMR is compatible with the use of a charge-coupled device camera, which has a slow operation time but allows the collection of temperature information over a wide area from a single measurement.[5,6] However, the temperature sensitivity of CW-ODMR is typically lower than that of pulsed-ODMR. Therefore, it is important to improve the temperature sensitivity of CW-ODMR for practical applications.

In this paper, we propose and demonstrate a method for measuring temperature using CW-ODMR with quantum spin states of NV centers dressed by a radio-frequency (RF) field under a transverse magnetic field.[26,27] The RF field is expected to improve the temperature sensitivity by suppressing the effects of strain and/or electric-field variations. We performed CW-ODMR measurements with RF fields under

transverse magnetic fields, and we showed experimentally that the linewidth decreases with increasing RF-field amplitude. From our experimental results, we estimated the theoretical sensitivity of the proposed scheme to be approximately $52.0 \pm 3.6\ \mathrm{mK}/\sqrt{\mathrm{Hz}}$, which is eight times better than that of the conventional scheme.[1,5,6,24] Furthermore, we experimentally measured the sensitivity by changing the temperature and obtained $50.4 \pm 3.5\ \mathrm{mK}/\sqrt{\mathrm{Hz}}$, which is close to the estimated value.

II. TEMPERATURE SENSING WITH RF-DRESSED STATES

A. Theoretical calculations

This section describes the physical properties of NV centers. The ground state of an NV center is a spin triplet, and its energy eigenstates are $|0\rangle$ and $|\pm 1\rangle$.[7,8] An NV center has four possible crystallographic axes, and these align with a nitrogen atom and a vacancy. When a magnetic field is applied parallel to the NV axis, the degenerate level $|\pm 1\rangle$ splits into $|+1\rangle$ and $|-1\rangle$. Conversely, when strain or transverse magnetic fields are applied, the degenerate level splits into two states defined as $|D\rangle = (|+1\rangle - |-1\rangle)/\sqrt{2}$ and $|B\rangle = (|+1\rangle + |-1\rangle)/\sqrt{2}$.[25–30] The spin states can be initialized to $|0\rangle$ by applying a green laser to the NV centers. Moreover, the spin state can be determined from the difference in the number of photons emitted from the NV centers. In addition, the spin state of an NV center can be controlled by applying a resonant MW field.[31,32] Therefore, by sweeping the MW frequency while simultaneously applying a green laser and an MW field, we can change the emitted photons and can thus find the resonance frequencies between $|0\rangle$ and the other energy eigenstates (CW-ODMR). Under the effect of strain or a transverse magnetic field, a transition between $|D\rangle$ and $|B\rangle$ can be induced by applying a resonant RF field.[26,27] In this case, the states $|D\rangle$ and $|B\rangle$ are split into other states dressed by the RF field, as shown in Fig. 1(a). These RF-dressed states can be observed by measuring the CW-ODMR spectrum in the presence of an RF field.

The Hamiltonian of an NV center with MW and RF fields is described as:[26,27]

$$H_{\mathrm{NV}} = D\hat{S}_z^2 + E_x(\hat{S}_x^2 - \hat{S}_y^2) + E_y(\hat{S}_x\hat{S}_y + \hat{S}_y\hat{S}_x) + \gamma_e B_x \hat{S}_x + \sum_{j=x,y,z}\left(\gamma_e B_{\mathrm{MW}}^{(j)}\hat{S}_j\cos(\omega_{\mathrm{MW}}t) + \gamma_e B_{\mathrm{RF}}^{(j)}\hat{S}_j\cos(\omega_{\mathrm{RF}}t)\right), \tag{1}$$

where $\hat{S}$ is the spin-1 operator of the electronic spin, D is the zero-field splitting, E_x (E_y) is the strain or electric field along the x (y) direction, γ_e is the gyromagnetic ratio of the electron spin, B_x is the transverse magnetic field, B_{MW} (B_{RF}) is the amplitude of the MW (RF) field, and ω_{MW} (ω_{RF}) is the MW (RF) field frequency. Under the condition $D \gg \gamma_e B_x \gg E_y$, we

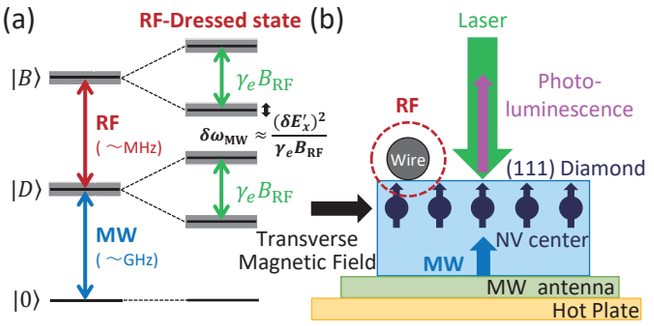

FIG. 1. (a) Energy diagram of our system. The NV centers are driven by radio-frequency (RF) and microwave (MW) fields to generate the RF-dressed states. Here, B_{RF} denotes the amplitude of the RF field, γ_e denotes the gyromagnetic ratio, $\delta\omega_{\mathrm{MW}}$ denotes the resonant frequency fluctuations, and $\delta E_x'$ denotes the strain (or electric-field) variations. (b) Experimental setup to measure CW-ODMR spectrum with an RF field under a transverse magnetic field.

can rewrite the Hamiltonian as

$$H_{\mathrm{NV}} \simeq D'\hat{S}_z^2 + E_x'(\hat{S}_x^2 - \hat{S}_y^2) + \sum_{j=x,y,z}\left(\gamma_e B_{\mathrm{MW}}^{(j)}\hat{S}_j\cos(\omega_{\mathrm{MW}}t) + \gamma_e B_{\mathrm{RF}}^{(j)}\hat{S}_j\cos(\omega_{\mathrm{RF}}t)\right), \tag{2}$$

where

$$D' = D + \frac{3}{2}\frac{(\gamma_e B_x)^2}{D+E_x}, \quad E_x' = E_x + \frac{1}{2}\frac{(\gamma_e B_x)^2}{D+E_x}. \tag{3}$$

Importantly, this analysis shows that the transverse magnetic field increases the effective strain or electric field from E_x to E_x'. Moving to a rotating frame defined by $U = \omega_{\mathrm{RF}}|B\rangle\langle B| - \omega_{\mathrm{MW}}|0\rangle\langle 0|$, we use the rotating-wave approximation, and the effective Hamiltonian is then described as

$$\begin{aligned} H_{\mathrm{NV}} \simeq\ & (D' + E_x' - \omega_{\mathrm{MW}} - \omega_{\mathrm{RF}})|B\rangle\langle B| \\ & + (D' - E_x' - \omega_{\mathrm{MW}})|D\rangle\langle D| \\ & + \frac{1}{2}i\gamma_e B_{\mathrm{MW}}^{(y)}(|0\rangle\langle D| - |D\rangle\langle 0|) \\ & + \frac{1}{2}\gamma_e B_{\mathrm{RF}}^{(z)}(|B\rangle\langle D| + |D\rangle\langle B|). \end{aligned} \tag{4}$$

If the drive is weak, the number of excitations of the NV centers will be small. In this case, we can treat the system as a harmonic oscillator,[30,33] so the Hamiltonian can be written as

$$H_{\mathrm{NV}} = \omega_b\hat{b}\hat{b}^\dagger + \omega_d\hat{d}\hat{d}^\dagger + i\lambda_d(\hat{d} - \hat{d}^\dagger) + J(\hat{b}^\dagger\hat{d} + \hat{b}\hat{d}^\dagger), \tag{5}$$

where $\omega_b = D' + E_x' - \omega_{\mathrm{MW}} - \omega_{\mathrm{RF}}$, $\omega_d = D' - E_x' - \omega_{\mathrm{MW}}$, $\lambda_d = \frac{1}{2}\gamma_e B_{\mathrm{MW}}^{(y)}$, and $J = \frac{1}{2}\gamma_e B_{\mathrm{RF}}^{(z)}$. The Heisenberg equation is then written as

$$\frac{\partial}{\partial t}\hat{b} = -i\omega_b\hat{b} - iJ\hat{d} - \Gamma_b\hat{b}, \tag{6}$$

$$\frac{\partial}{\partial t}\hat{d} = -i\omega_d\hat{d} - \lambda_d - iJ\hat{b} - \Gamma_d\hat{d}, \tag{7}$$

where Γ_b (Γ_d) are the decay rates of states $|B\rangle$ ($|D\rangle$). In CW-ODMR, the system reaches a steady state, and we can thus set $\frac{\partial}{\partial t}\hat{b} = \frac{\partial}{\partial t}\hat{d} = 0$. We can therefore obtain an analytical solution to fit the shape of the CW-ODMR spectrum as follows:

$$f = 1 - \frac{\lambda_d^2\left(\Gamma_b^2 + \omega_b^2\right)}{J^4 + 2J^2(\Gamma_b\Gamma_d - \omega_b\omega_d) + \left(\Gamma_b^2 + \omega_b^2\right)\left(\Gamma_d^2 + \omega_d^2\right)}. \tag{8}$$

This type of function has been used to reproduce CW-ODMR spectra in previous studies.[27,29,30,34] Moreover, sharp dips will appear in this spectrum in the presence of a transverse magnetic field or in the absence of any magnetic field,[26,27,29,30,34,35] and this function can be used to fit the shape of the spectrum.

We now explain the why the RF-dressed states are robust against strain or electric-field variations. From the above expressions, we can calculate the MW resonance frequency as

$$\omega_{\mathrm{MW0}} = \frac{1}{2}\left[2D' \pm \omega_{\mathrm{RF}} \pm \sqrt{(2E_x' - \omega_{\mathrm{RF}})^2 + \left(\gamma_e B_{\mathrm{RF}}^{(z)}\right)^2}\right]. \tag{9}$$

By setting $\omega_{\mathrm{RF}} = 2E_x'$, we generate RF-dressed states.[26,27] If there are strain or electric-field variations with inhomogeneous width $\delta E_x'$, then the resonance frequency will fluctuate. We then obtain

$$\begin{aligned}\omega_{\mathrm{MW}} &= \omega_{\mathrm{MW0}} + \delta\omega_{\mathrm{MW}} \\ &= \frac{1}{2}\left[2D' \pm \omega_{\mathrm{RF}} \pm \sqrt{(\delta E_x')^2 + \left(\gamma_e B_{\mathrm{RF}}^{(z)}\right)^2}\right],\end{aligned} \tag{10}$$

where $\delta\omega_{\mathrm{MW}}$ is the width of the fluctuations. When the RF-field amplitude ($\gamma_e B_{\mathrm{RF}}^{(z)}$) is sufficiently larger than the inhomogeneous width ($\delta E_x'$), we can use a Taylor expansion to obtain

$$\delta\omega_{\mathrm{MW}} \simeq \frac{1}{4}\frac{(\delta E_x')^2}{\gamma_e B_{\mathrm{RF}}^{(z)}}. \tag{11}$$

This shows that, by increasing $B_{\mathrm{RF}}^{(z)}$, we can suppress the effects of strain and electric-field variations; the linewidth in CW-ODMR will be decreased, and this should in turn improve the temperature sensitivity.

B. Temperature sensitivity

Here, we describe our scheme for estimating the temperature by using CW-ODMR with RF-dressed states. By performing CW-ODMR measurements under the application of an RF field and a transverse magnetic field, the RF-dressed states become observable. We propose using the resonance frequencies of these states to measure temperature. As the temperature increases, the resonance frequency will shift because of a change in the zero-field splitting[9] of -74.2 kHz/K, which should be detectable using CW-ODMR measurements. In our experiments, we found that the RF-dressed states were robust against electric-field noise. We confirmed that as we increased the amplitude of the RF field, the linewidths of the dips corresponding to the RF-dressed states decreased. From the experimental results of the CW-ODMR measurements, we can calculate the sensitivity of the temperature sensor as

$$\delta T = \frac{\delta C}{(\delta C/\delta\nu)(\delta\nu/\delta T)}, \tag{12}$$

where δC is the standard deviation of the contrast, $\delta C/\delta\nu$ is the linear slope of the dip in the CW-ODMR spectrum, and $\delta\nu/\delta T$ is the frequency shift of the NV center with respect to temperature.

Moreover, changing the temperature of the NV centers will also lead to measurement of the system's temperature sensitivity. This is because the CW-ODMR spectrum will be shifted by changes in temperature. We can thus obtain the temperature sensitivity from a change in the contrast of the temperature at a fixed MW frequency, and we can therefore choose a specific MW frequency to maximize the sensitivity. In short, we can measure the temperature sensitivity using

$$\delta T = \frac{\delta C}{(\delta C/\delta T)}, \tag{13}$$

where $\delta C/\delta T$ denotes the derivative of the contrast with respect to temperature.

C. Experimental details

For the experiments, we used a home-built confocal laser scanning microscopy and excited the electron spin resonance of the NV centers using green laser (532 nm), MW, and RF fields [Fig. 1(b)]. The photoluminescence from the NV centers passed through a pinhole and was detected by an avalanche photodiode. The diamond sample was positioned above the antenna[36] that was used to emit the MW fields. We applied RF fields by placing a copper wire on the diamond sample and applying an AC voltage. The temperature was controlled to an accuracy of 0.1 K using a hot plate under the MW antenna. Considering the high thermal conductivity of diamond, the temperature of the NV centers was monitored by assuming that it was equal to the temperature of a thermocouple placed on the upper surface of the MW antenna. A diamond sample with an NV layer was grown by nitrogen-doped chemical vapor deposition on a (111)-oriented diamond substrate. The NV axis in the diamond was preferentially aligned normal to the substrate.[37–40] The density of the NV centers was estimated to be 10^{16} /cm^3.

III. RESULTS AND DISCUSSION

We performed CW-ODMR experiments with MW and RF fields under the effect of a transverse magnetic field; the frequency of the applied RF field was 10.5 MHz. The results of these experiments are shown in Fig. 2(a). The contrast in the ODMR spectrum depends on the relationship between the MW polarization and the direction of the strain.[41]

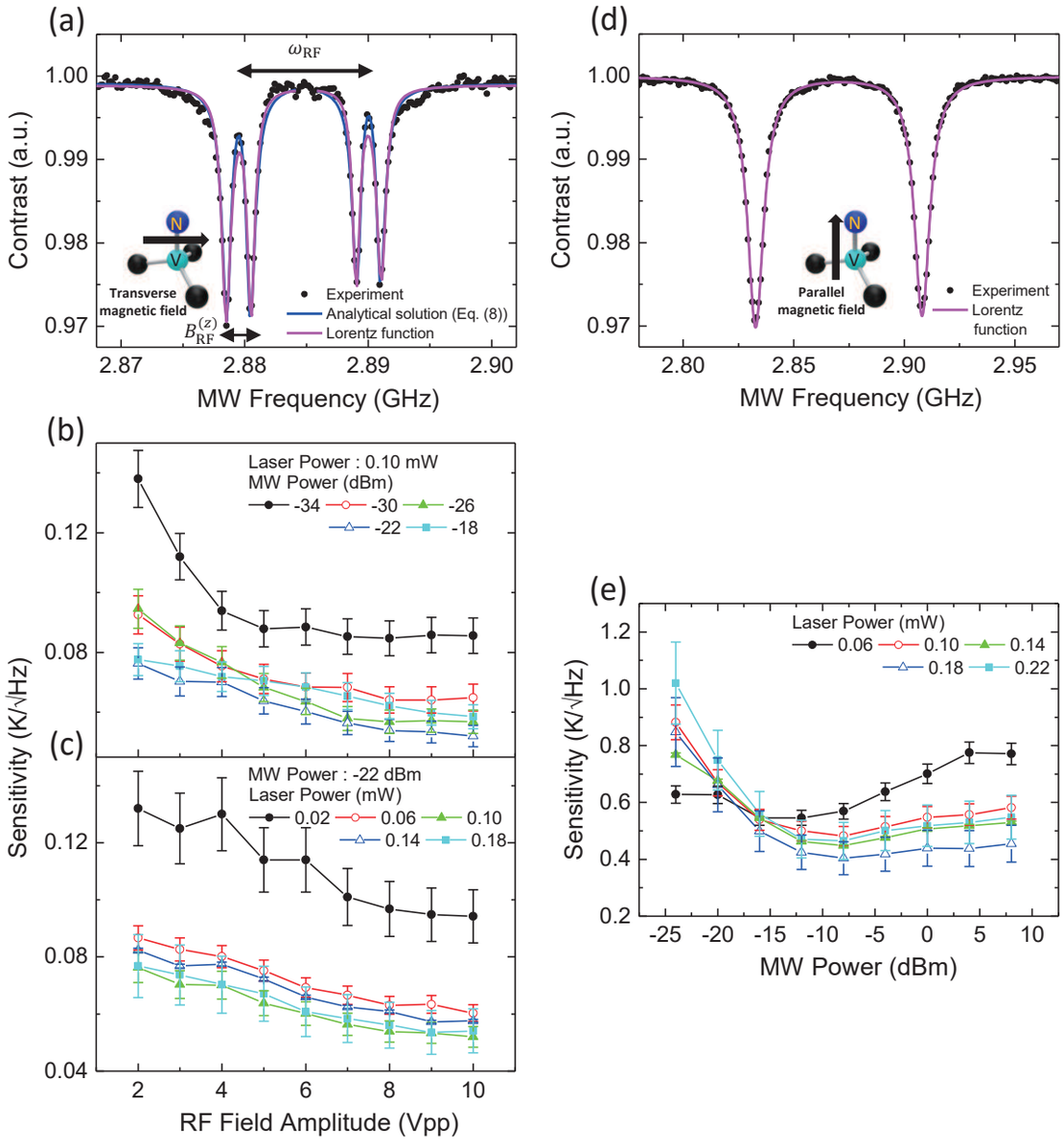

FIG. 2. (a) Experimental results of CW-ODMR measurements with MW and RF fields under a transverse magnetic field. The MW frequency was swept from 2.868 to 2.902 GHz, and an RF field was applied with a frequency of 10.5 MHz. The experimental results were fitted to a multiple Lorentzian function (magenta) and with the analytical solution Eq. (8) (blue). The inset shows the orientation of the NV centers and the direction of the magnetic field. (b) Dependence of the temperature sensitivity on the MW power and RF amplitude as calculated from CW-ODMR measurements; the laser power was fixed at around 0.10 mW. (c) Dependence of the temperature sensitivity on the laser power and RF amplitude calculated from CW-ODMR measurements with MW and RF fields; the MW power was fixed at −22 dBm. (d) Experimental results of CW-ODMR measurements with MW field under a parallel magnetic field; the MW frequency was swept from 2.780 to 2.970 GHz. The experimental results were fitted to Lorentzian functions (magenta). The inset shows the orientation of the NV centers and the direction of the magnetic field. (e) Dependence of the temperature sensitivity on the laser and MW power calculated from CW-ODMR measurements with an MW field.

In our case, the contrast to drive the $|D\rangle$ state becomes larger than that to drive the $|B\rangle$ state. Based on the four dips observed in the CW-ODMR spectra, we confirmed that RF-dressed states were generated; the combination of magnetic-field noise and strain variations induces sharp dips in CW-ODMR spectra.[26,27,29,30,34] Although we tried to fit the results using a multiple Lorentz function, because of these sharp dips, this did not accurately reproduce the experimental results. Thus, we instead used Eq. (8) to fit the results, and this led to good agreement.

By changing the laser power, MW power, and RF power, we further investigated the dependence of the CW-ODMR spectrum on these parameters. By fitting the experimental results using Eq. (8), we calculated the sensitivity of the system as a temperature sensor. In this calculation, we considered the linear slope of the dip in the CW-ODMR spectrum and the standard deviation of the count rate of emitted photons. Figure 2(b) shows how the sensitivity depends on the MW and RF amplitudes with the laser power fixed around 0.10 mW. As the MW power was increased, the contrast improved, but the linewidth increased. This shows a trade-off relationship between the contrast and the linewidth. Therefore, there is an optimal MW power, and this was found to be -22 dBm from Fig. 2(b). However, as illustrated in Fig. 2(c), when we fixed the MW power to about -22 dBm, the laser power and RF amplitude also affected the sensitivity. As we increased the laser power, the contrast decreased while the standard deviation of the contrast improved. Thus, the laser power should be adjusted to optimize the sensitivity.

From these results, we determined the optimal conditions for the laser power (0.10 mW), MW power (-22 dBm), and RF amplitude (10 Vpp) and obtained a sensitivity of 52.0 ± 3.6 mK$/\sqrt{\text{Hz}}$. For these results, we used the standard deviation of contrast $\delta C = (1.93 \pm 0.13) \times 10^{-4}\ /\sqrt{\text{Hz}}$ considering the standard error, the linear slope of the dip in CW-ODMR spectrum $\delta C/\delta\nu = 5.00 \times 10^{-8}$/Hz, and the zero-field splitting $\delta\nu/\delta T = -74.2$ kHz/K.

For comparison, we performed CW-ODMR experiments with a parallel magnetic field. This is a typical approach for measuring temperature using the CW-ODMR method. Figure 2(d) shows the results of these measurements. In addition, by changing the laser and MW power, we investigated how the CW-ODMR spectrum depends on these parameters with a parallel magnetic field. By fitting the experimental results to a Lorentzian, we calculated the sensitivity of the temperature sensor by taking into account the standard deviation of the photon count rate. Figure 2(e) shows how the sensitivity depends on the laser and MW power. From these results, we found optimal values for the laser power (0.10 mW) and MW power (-8 dBm), and we obtained a sensitivity of approximately 404 ± 57.8 mK$/\sqrt{\text{Hz}}$. For this calculation, we used $\delta C = (1.34 \pm 0.19) \times 10^{-4}/\sqrt{\text{Hz}}$, $\delta C/\delta\nu = 4.47 \times 10^{-9}$/Hz, and $\delta\nu/\delta T = -74.2$ kHz/K. This sensitivity is approximately one eighth that of the proposed scheme.

We also measured the sensitivity under the same conditions used for Figs. 2(a) and 2(d), respectively, when the temperature was actually changed. First, we confirmed that the CW-ODMR spectrum shifts in both cases when the temperature changes, as illustrated in Figs. 3(a) and 3(c). Figure 3(b) shows the changes in contrast at an MW frequency of 2.87841 GHz when the temperature was increased in 0.2 K steps with RF-dressed states created under a transverse magnetic field. We obtained a sensitivity of 50.4 ± 3.5 mK$/\sqrt{\text{Hz}}$ using $\delta C = (1.93 \pm 0.13) \times 10^{-4}/\sqrt{\text{Hz}}$ and $\delta C/\delta T = 3.83 \times 10^{-3}$/K. For comparison, Fig. 3(d) shows the changes in the contrast at an MW frequency of 2.83542 GHz when the temperature was increased in 5 K steps under a parallel magnetic field. Here, we obtained a sensitivity of 415 ± 59.4 mK$/\sqrt{\text{Hz}}$ using $\delta C = (1.34 \pm 0.19) \times 10^{-4}/\sqrt{\text{Hz}}$ and $\delta C/\delta T = 3.23 \times 10^{-4}$/K. These measured sensitivities are very close to the estimated values. The sensitivity of the proposed scheme is thus eight times that of the conventional scheme. These results show the advantage of using a temperature sensor with RF-dressed states.

We now discuss the origin of the improved sensitivity that is obtained using the proposed scheme. The linewidths under a transverse magnetic field are estimated to be 2.15 and 1.80 MHz for MW powers of -18 and -22 dBm in the absence of an RF field. For comparison, the linewidths were estimated to be 6.46 and 6.29 MHz for MW powers of -20 and -24 dBm under a parallel magnetic field. This indicates that transverse magnetic fields suppress the magnetic-field noise from P1 centers, and that the linewidth decreases about threefold under a transverse magnetic field.[42] The RF-dressed states also become robust to noise; as explained above, the effects of variations of strain and/or electric field can be suppressed by applying an RF field. As the amplitude of the RF field is increased, the linewidths of the peaks decrease, as shown in Fig. 4. Based on the analytical expression of the linewidth in Eq. (11), we can fit the linewidth of the peaks against the RF amplitude in Fig. 4. More specifically, we use

$$\delta\omega_{\text{MW}} = \frac{1}{4}\frac{(\delta E_x')^2}{\gamma_e B_{\text{RF}}^{(z)}} + \delta\omega_{\text{MW:others}} \tag{14}$$

for the fitting, where $\delta\omega_{\text{MW:others}}$ is the linewidth derived from noise other than strain (electric-field) variations, including randomized magnetic fields, zero-field splitting variations, homogeneous widths, and longitudinal relaxation. There is good agreement between the theoretical and experimental values, and this indicates that the RF actually suppresses the strain (electric-field) variations. This is the reason for the improved temperature sensitivity of the proposed scheme.

Let us compare our scheme with another scheme for measuring the temperature using CW-ODMR. An innovative approach to measuring the temperature with high sensitivity using hyperfine transitions has been proposed.[43] However, in this scheme, to drive the hyperfine transitions, the linewidth of the ODMR should be much smaller than the hyperfine coupling strength of 2.3 MHz. Therefore, a diamond sample with a low NV density should be used because otherwise it will not be possible to resolve the hyperfine splitting. However, using our scheme, it is not necessary to resolve the hyperfine splitting. This shows that, if a high density of NV centers is available, our scheme will be more advantageous than this scheme.

IV. CONCLUSION

In this paper, we describe a method for measuring temperature using CW-ODMR with a quantum state dressed by an RF field under a transverse magnetic field. Because the presence of an RF field suppresses the effect of inhomogeneous broadening due to strain and/or electric-field variations, the sensitivity of this technique is better than that of the conventional

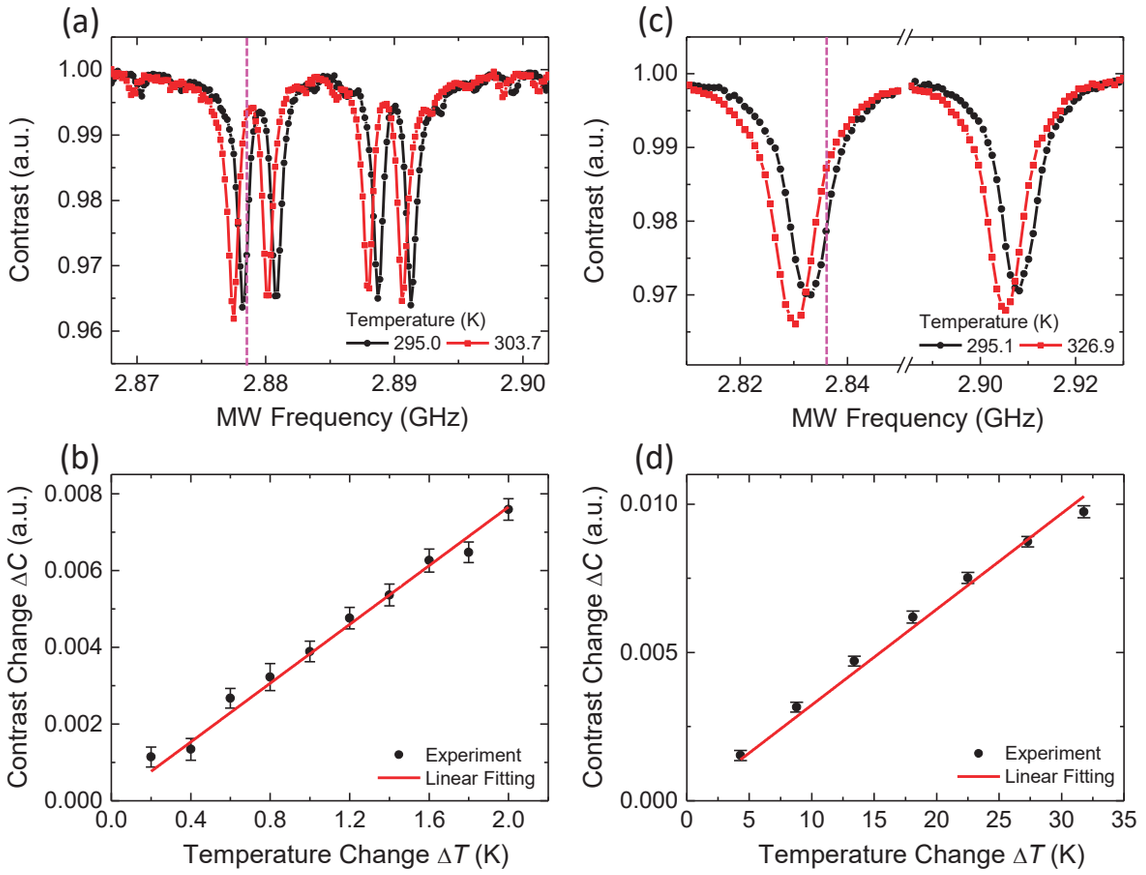

FIG. 3. (a) CW-ODMR spectra for different temperatures and (b) changes in contrast at an MW frequency of 2.87841 GHz as the temperature was increased in 0.2 K steps with an RF field and a transverse magnetic field. (c) CW-ODMR spectra for different temperatures and (d) changes in contrast at an MW frequency of 2.83542 GHz as the temperature was increased in 5 K steps under a parallel magnetic field.

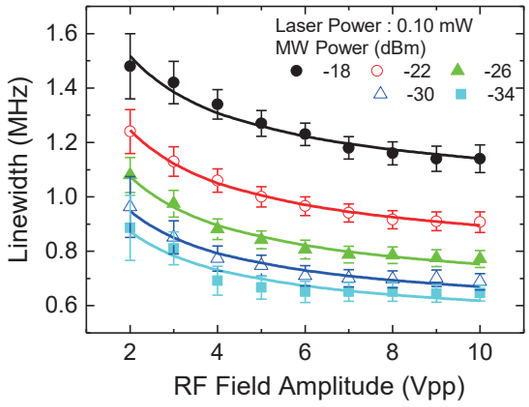

FIG. 4. Changes in the linewidth of CW-ODMR spectra with varying MW and RF fields under a transverse magnetic field.

scheme. Moreover, the presence of a transverse magnetic field suppresses the magnetic-field noise, and this also contributes to improving the sensitivity. We experimentally measured the temperature sensitivity of this system and obtained a value of $50.4 \pm 3.5\ \mathrm{mK}/\sqrt{\mathrm{Hz}}$; this is eight times better than that of the conventional scheme. These results show the practicality of using a temperature sensor with RF-dressed states.

ACKNOWLEDGMENTS

This work was supported by MEXT Q-LEAP (Grant No. JPMXS0118067395), MEXT KAKENHI (Grants No. 18H01502, 20H05661, 22H01558), and CSRN, Keio University. This work was supported by Leading Initiative for Excellent Young Researchers MEXT Japan and JST presto (Grant No. JPMJPR1919) Japan and Kanazawa University CHOZEN Project 2022.

AUTHOR DECLARATIONS

Conflict of Interest

The authors declare no conflicts of interest.

DATA AVAILABILITY

Data underlying the results presented in this paper are not publicly available at this time but may be obtained from the authors upon reasonable request.

[1]H. An, Z. Yin, C. Mitchell, A. Semnani, A. R. Hajrasouliha, and M. Hosseini, Meas. Sci. Technol. **32**, 015701 (2021).
[2]G. Kucsko, P. C. Maurer, N. Y. Yao, M. Kubo, H. J. Noh, P. K. Lo, H. Park, and M. D. Lukin, Nature **500**, 54–58 (2013).
[3]H. Yukawa, M. Fujiwara, K. Kobayashi, Y. Kumon, K. Miyaji, Y. Nishimura, K. Oshimi, Y. Umehara, Y. Teki, T. Iwasaki, M. Hatano, H. Hashimoto, and Y. Baba, Nanoscale Adv. **2**, 1859–1868 (2020).
[4]P. Andrich, J. Li, X. Liu, F. J. Heremans, P. F. Nealey, and D. D. Awschalom, Nano Lett. **18**, 4684–4690 (2018).
[5]Y. Chen, Z. Li, H. Guo, D. Wu, and J. Tang, EPJ Quantum Technol. **8**, 1 (2021).
[6]C. Foy, L. Zhang, M. E. Trusheim, M. E. Trusheim, K. R. Bagnall, M. Walsh, M. Walsh, E. N. Wang, D. R. Englund, and D. R. Englund, ACS Appl. Mater. Interfaces **12**, 26525–26533 (2020).
[7]M. W. Doherty, N. B. Manson, P. Delaney, F. Jelezko, J. Wrachtrup, and L. C. L. Hollenberg, Phys. Rep. **528**, 1–45 (2013).
[8]L. Rondin, J. P. Tetienne, T. Hingant, J. F. Roch, P. Maletinsky, and V. Jacques, Rep. Prog. Phys. **77**, 056503 (2014).
[9]V. M. Acosta, E. Bauch, M. P. Ledbetter, A. Waxman, L. S. Bouchard, and D. Budker, Phys. Rev. Appl. **104**, 070801 (2010).
[10]G. Balasubramanian, P. Neumann, D. Twitchen, M. Markham, R. Kolesov, N. Mizuochi, J. Isoya, J. Achard, J. Beck, J. Tissler, V. Jacques, P. R. Hemmer, F. Jelezko, and J. Wrachtrup, Nat. Mater. **8**, 383–387 (2009).
[11]H. Morishita, T. Tashima, D. Mima, H. Kato, T. Makino, S. Yamasaki, M. Fujiwara, and N. Mizuochi, Sci. Rep. **9**, 13318 (2019).
[12]E. D. Herbschleb, H. Kato, Y. Maruyama, T. Danjo, T. Makino, S. Yamasaki, I. Ohki, K. Hayashi, H. Morishita, M. Fujiwara, and N. Mizuochi, Nat. Commun. **10**, 3766 (2019).
[13]G. Balasubramanian, I. Y. Chan, R. Kolesov, M. Al-Hmoud, J. Tisler, C. Shin, C. Kim, A. Wojcik, P. R. Hemmer, A. Krueger, T. Hanke, A. Leitenstorfer, R. Bratschitsch, F. Jelezko, and J. Wrachtrup, Nature **455**, 648–651 (2008).
[14]J. P. Tetienne, A. Lombard, D. A. Simpson, C. Ritchie, J. Lu, P. Mulvaney, and L. C. Hollenberg, Nano Lett. **16**, 326–333 (2016).
[15]K. Chang, A. Eichler, J. Rhensius, L. Lorenzelli, and C. L. Degen, Nano Lett. **17**, 2367–2373 (2017).
[16]M. Fukami, C. G. Yale, P. Andrich, X. Liu, F. J. Heremans, P. F. Nealey, and D. D. Awschalom, Phys. Rev. Appl. **12**, 014042 (2019).
[17]M. Fujiwara and Y. Shikano, Nanotechnology **32**, 482002 (2021).
[18]G. Q. Liu, X. Feng, N. Wang, Q. Li, and R. B. Liu, Nat. Commun. **10**, 1344 (2019).
[19]J. M. Taylor, P. Cappellaro, L. Childress, L. Jiang, D. Budker, P. R. Hemmer, A. Yacoby, R. Walsworth, and M. D. Lukin, Nat. Phys. **4**, 810–816 (2008).
[20]S. Choe, J. Yoon, M. Lee, J. Oh, D. Lee, H. Kang, C. H. Lee, and D. Lee, Curr. Appl. Phys. **18**, 1066–1070 (2018).
[21]P. Neumann, I. Jakobi, F. Dolde, C. Burk, R. Reuter, G. Waldherr, J. Honert, T. Wolf, A. Brunner, J. H. Shim, D. Suter, H. Sumiya, J. Isoya, and J. Wrachtrup, Nano Lett. **13**, 2738–2742 (2013).
[22]D. M. Toyli, C. F. De Las Casas, D. J. Christle, V. V. Dobrovitski, and D. D. Awschalom, Proc. Natl. Acad. Sci. U.S.A. **110**, 8417–8421 (2013).
[23]J. Wang, F. Feng, J. Zhang, J. Chen, Z. Zheng, L. Guo, W. Zhang, X. Song, G. Guo, L. Fan, C. Zou, L. Lou, W. Zhu, and G. Wang, Phys. Rev. B **91**, 155404 (2015).
[24]Y. K. Tzeng, P. C. Tsai, H. Y. Liu, O. Y. Chen, H. Hsu, F. G. Yee, M. S. Chang, and H. C. Chang, Nano Lett. **15**, 3945–3952 (2015).
[25]J. Yun, K. Kim, S. Park, and D. Kim, Adv. Quantum Technol. **4**, 2100084 (2021).
[26]S. Saijo, Y. Matsuzaki, S. Saito, T. Yamaguchi, I. Hanano, H. Watanabe, N. Mizuochi, and J. Ishi-Hayase, Appl. Phys. Lett. **113**, 082405 (2018).
[27]T. Yamaguchi, Y. Matsuzaki, S. Saito, S. Saijo, H. Watanabe, N. Mizuochi, and J. Ishi-Hayase, Jpn. J. Appl. Phys. **58**, 100901 (2019).
[28]K. Fang, V. M. Acosta, C. Santori, Z. Huang, K. M. Itoh, H. Watanabe, S. Shikata, and R. G. Beausoleil, Phys. Rev. Lett. **110**, 1–5 (2013).
[29]X. Zhu, Y. Matsuzaki, R. Amsüss, K. Kakuyanagi, T. Shimo-Oka, N. Mizuochi, K. Nemoto, K. Semba, W. J. Munro, and S. Saito, Nat. Commun. **5**, 3524 (2014).
[30]Y. Matsuzaki, H. Morishita, T. Shimooka, T. Tashima, K. Kakuyanagi, K. Semba, W. J. Munro, H. Yamaguchi, N. Mizuochi, and S. Saito, J. Phys.: Condens. Matter **28**, 275302 (2016).
[31]A. Dréau, M. Lesik, L. Rondin, P. Spinicelli, O. Arcizet, J.-F. Roch, and V. Jacques, Phys. Rev. B **84**, 195204 (2011).
[32]K. Jensen, V. M. Acosta, A. Jarmola, and D. Budker, Phys. Rev. B **87**, 014115 (2013).
[33]I. Diniz, S. Portolan, R. Ferreira, J. M. Gérard, P. Bertet, and A. Auffèves, Phys. Rev. A **84**, 063810 (2011).
[34]K. Hayashi, Y. Matsuzaki, T. Taniguchi, T. Shimo-Oka, I. Nakamura, S. Onoda, T. Ohshima, H. Morishita, M. Fujiwara, S. Saito, and N. Mizuochi, Phys. Rev. Appl. **10**, 034009 (2018).
[35]A. K. Dmitriev, H. Y. Chen, G. D. Fuchs, and A. K. Vershovskii, Phys. Rev. A **100**, 011801 (2019).
[36]K. Sasaki, Y. Monnai, S. Saijo, R. Fujita, H. Watanabe, J. Ishi-Hayase, K. M. Itoh, and E. Abe, Rev. Sci. Instrum. **87**, 053904 (2016).
[37]H. Ishiwata, M. Nakajima, K. Tahara, H. Ozawa, T. Iwasaki, and M. Hatano, Appl. Phys. Lett. **111**, 043103 (2017).
[38]T. Fukui, Y. Doi, T. Miyazaki, Y. Miyamoto, H. Kato, T. Matsumoto, T. Makino, S. Yamasaki, R. Morimoto, N. Tokuda, M. Hatano, Y. Sakagawa, H. Morishita, T. Tashima, S. Miwa, Y. Suzuki, and N. Mizuochi, Appl. Phys. Express **7**, 055201 (2014).
[39]M. Lesik, J. P. Tetienne, A. Tallaire, J. Achard, V. Mille, A. Gicquel, J. F. Roch, and V. Jacques, Appl. Phys. Lett. **104**, 113107 (2014).
[40]J. Michl, T. Teraji, S. Zaiser, I. Jakobi, G. Waldherr, F. Dolde, P. Neumann, M. W. Doherty, N. B. Manson, J. Isoya, and J. Wrachtrup, Appl. Phys. Lett. **104**, 102407 (2014)
[41]H. Zheng, J. Xu, G. Z. Iwata, T. Lenz, J. Michl, B. Yavkin, K. Nakamura, H. Sumiya, T. Ohshima, J. Isoya, J. Wrachtrup, A. Wickenbrock, and D. Budker, Phys. Rev. Appl. **11**, 064068 (2019).
[42]C. S. Shin, C. E. Avalos, M. C. Butler, H. J. Wang, S. J. Seltzer, R. B. Liu, A. Pines, and V. S. Bajaj, Phys. Rev. B **88**, 161412 (2013).
[43]A. M. Wojciechowski, M. Karadas, C. Osterkamp, S. Jankuhn, J. Meijer, F. Jelezko, A. Huck, and U. L. Andersen, Appl. Phys. Lett. **113**, 013502 (2018).

Journal of Applied Physics

AIP Publishing

Journal of Applied Physics

AIP Publishing

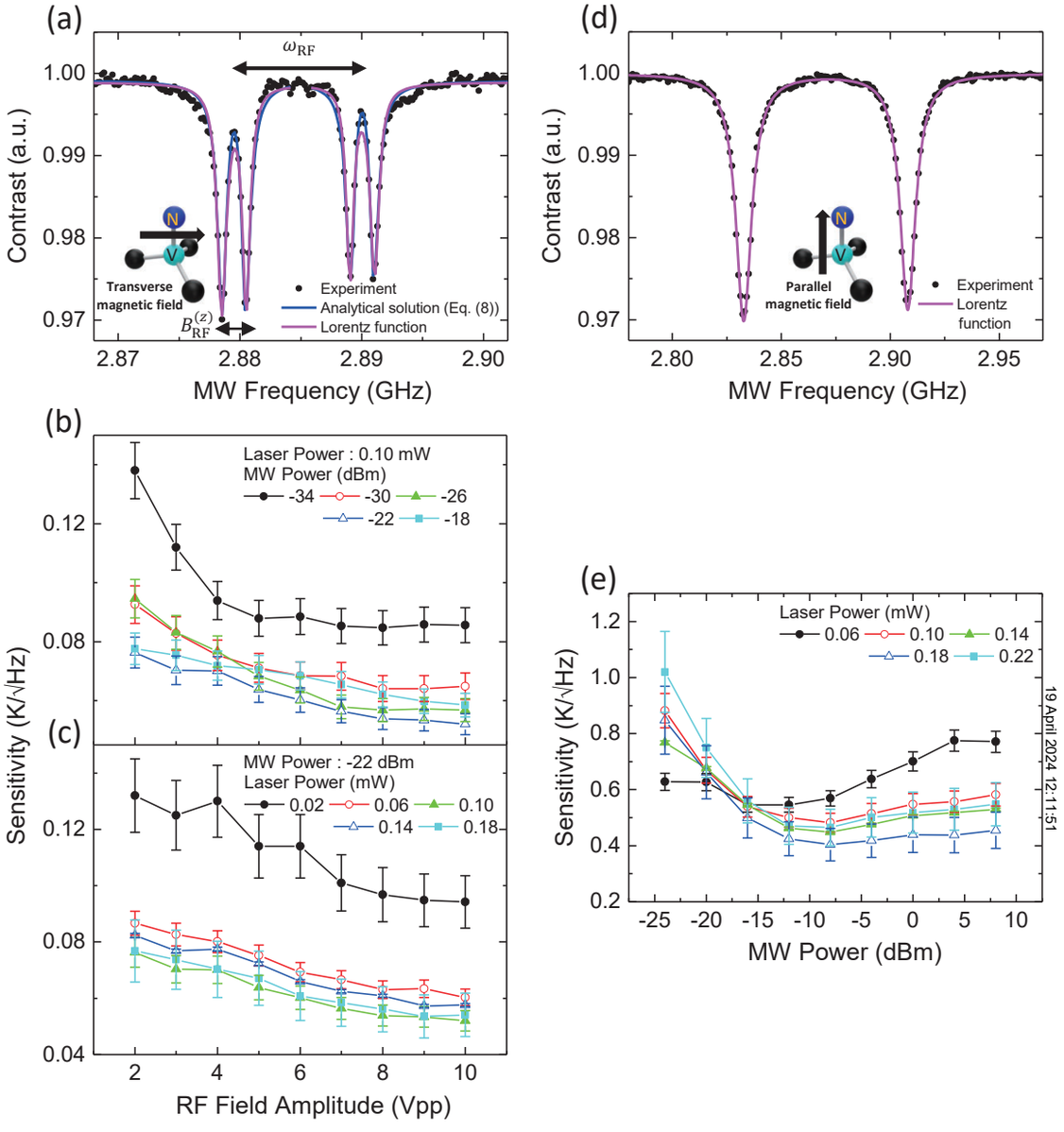

AIP Publishing

Journal of Applied Physics

ACCEPTED MANUSCRIPT

This is the author's peer reviewed, accepted manuscript. However, the online version of record will be different from this version once it has been copyedited and typeset.
PLEASE CITE THIS ARTICLE AS DOI: 10.1063/5.0129706

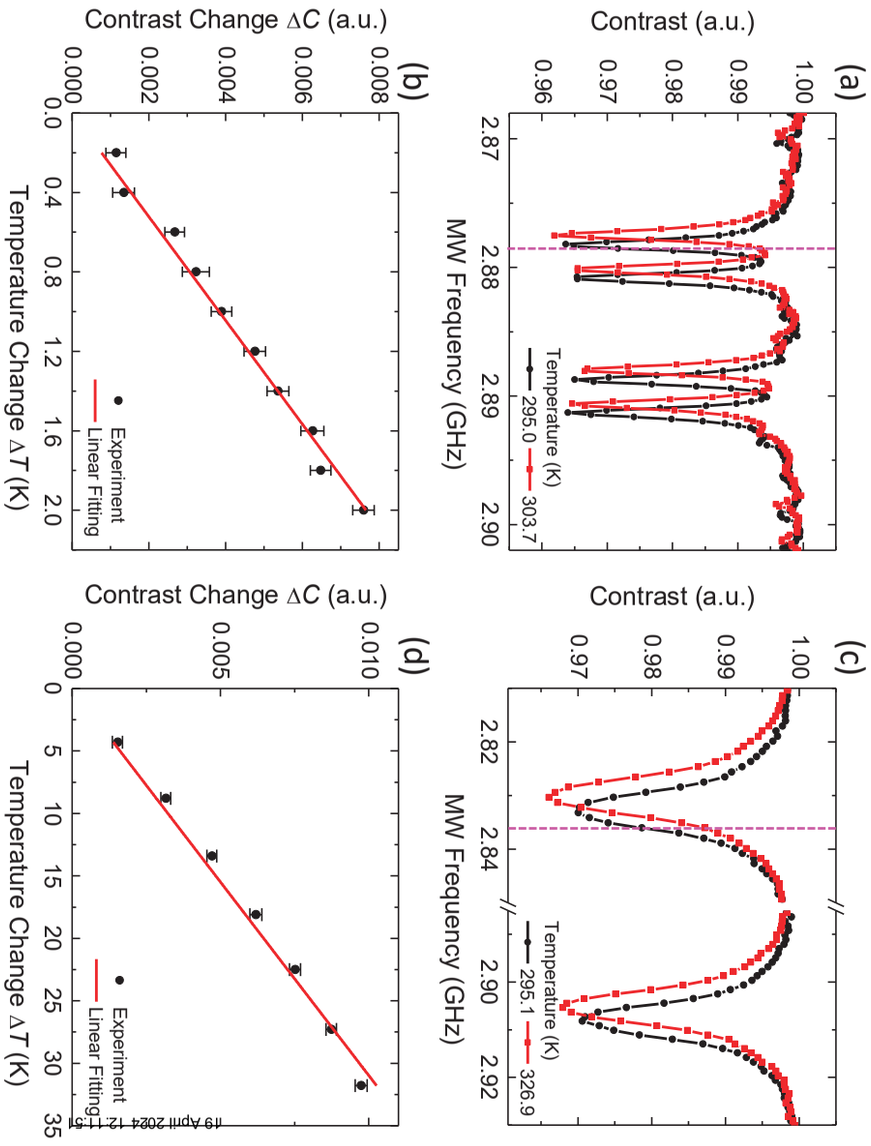

PLEASE CITE THIS ARTICLE AS DOI: 10.1063/5.0129706